International Journal of Heat and Technology
Vol. 44, No. 4, August, 2026, pp. 1553-1564
Journal homepage: http://iieta.org/journals/ijht

Hydrodynamic Effects of Porous-Net Density on Local Scour Reduction Around Cylindrical Bridge Piers

Hamzah Al Imran[1*], Abd Rakhim Nanda[1], Muhammad Faisal[2], Nenny[1], Muhammad Syafaat Kuba[1], Nurnawaty[1], Andi Makbul Syamsuri[1], Fatriady Mustakim Rusniah[1], Muhammad Agusalim[1]

[1] Department of Civil Engineering, Universitas Muhammadiyah Makassar, Makassar 90221, Indonesia
[2] Department of Informatics, Universitas Muhammadiyah Makassar, Makassar 90221, Indonesia

Corresponding Author Email: hamzah@unismuh.ac.id

Copyright: ©2026 The authors. This article is published by IIETA and is licensed under the CC BY 4.0 license (http://creativecommons.org/licenses/by/4.0/).

https://doi.org/10.18280/ijht.440419

Received: 3 June 2026
Revised: 13 August 2026
Accepted: 25 August 2026
Available online: 31 August 2026

Keywords:
local scour, cylindrical bridge pier, porous-net structure, flow-modifying, scour mitigation

ABSTRACT

Local scour around bridge piers is a major cause of foundation instability under strong hydraulic loading. This study experimentally evaluates porous-net configurations as flow-modifying countermeasures for reducing local scour around a cylindrical bridge pier. Controlled flume tests were conducted under two discharge conditions using an unprotected pier and two porous-net configurations with different relative densities and structural arrangements: a triangular configuration (MJB1) and a reinforced triangular configuration (MJB2). Flow velocity and dimensionless hydraulic parameters were evaluated together with maximum scour depth, scour volume, and spatial bed-elevation change. Unlike previous studies that primarily examined rigid permeable devices or assessed performance solely by maximum scour depth, this study applies a multi-metric morphological assessment to determine both the magnitude and spatial extent of scour mitigation. Under the higher tested discharge condition (Q_2), the reinforced MJB2 configuration reduced the maximum scour depth from approximately 5.4 cm for the unprotected pier to 0.9 cm, corresponding to an 83.36% reduction. This result was obtained under the specified laboratory conditions ($D = 0.05$ m, $h = 0.15$ m, and $d_{50} = 0.80$ mm) and should be interpreted within this experimental context. The measured velocity attenuation and morphological response indicate that the denser configuration increased hydraulic resistance and limited sediment entrainment near the pier. The results indicate that the porous-net configuration and relative structural density influenced scour-mitigation performance under the investigated laboratory conditions. The proposed multi-metric evaluation provides a more comprehensive basis for assessing flexible porous countermeasures than maximum scour depth alone.

1. INTRODUCTION

Local scour around bridge piers is widely recognized as one of the most critical hydraulic processes affecting the stability and safety of bridge foundations in river environments [1]. When an approaching flow encounters a cylindrical bridge pier, the flow field becomes highly disturbed, producing complex three-dimensional turbulent structures, including downflow jets, horseshoe vortices at the pier's upstream base, and wake vortices downstream [2]. These hydrodynamic structures significantly intensify the bed shear stress around the pier and increase the flow's sediment transport capacity, resulting in progressive erosion of the riverbed surrounding the pier foundation. Excessive scour depth may expose bridge foundations and ultimately threaten the bridge's structural integrity.

The mechanism of local scour around cylindrical obstacles has been widely investigated in hydraulic engineering research. When flow impinges on a bridge pier, stagnation pressure at the upstream face generates a downward jet that deflects toward the bed and forms a horseshoe vortex system around the base of the structure [3]. This vortex system plays a dominant role in lifting and transporting sediment particles from the bed. In addition, flow contraction along the sides of the pier accelerates the local velocity and further increases the bed shear stress, while wake vortices downstream redistribute sediment and contribute to the expansion of the scour hole.

Because excessive scour poses a major threat to bridge safety, numerous countermeasures have been developed to mitigate sediment erosion around bridge foundations [4]. Conventional protection methods typically involve structural armoring of the riverbed, such as riprap layers, concrete collars, geotextile mattresses, or sacrificial piles installed around the pier. These techniques primarily function by increasing the bed material's resistance to erosion or by shielding the foundation from high-velocity flow. Although these structural countermeasures are widely used in engineering practice, they often require large quantities of construction materials, involve complex installation procedures, and may significantly alter natural river morphology and sediment transport processes [5].

To address these limitations, recent studies have

increasingly explored alternative strategies that modify the hydrodynamic characteristics of the approaching flow rather than directly reinforcing the riverbed [6]. Flow-modifying structures, such as current deflectors, flow-guiding devices, and porous barriers, have been proposed to reduce the intensity of vortex systems responsible for scour formation [7]. By redistributing the velocity field and attenuating turbulence around the pier, these structures can reduce near-bed shear stress and consequently limit sediment entrainment. Among these alternatives, porous structures are particularly attractive because they can dissipate hydraulic energy while allowing partial flow passage. Unlike impermeable barriers, which produce strong flow separation and turbulent amplification, porous obstacles allow a fraction of the incoming flow to pass through their internal voids [8]. This bleed flow reduces the pressure gradient at the upstream face of the obstacle and weakens the formation of strong horseshoe vortices near the bed, thereby limiting sediment entrainment and reducing scour intensity. Furthermore, the hydraulic performance of porous obstacles is strongly influenced by their structural porosity or density. Variations in porosity modify the velocity distribution and bed shear stress in the surrounding flow field. Increasing the obstacle's porosity allows more flow to pass through the structure, reducing the flow velocity beneath the obstacle and, consequently, decreasing the resulting scour depth [9]. Numerical and theoretical analyses have demonstrated that higher porosity can significantly reduce the maximum scour depth beneath hydraulic obstacles by lowering the bed shear stress acting on the sediment bed.

Despite increasing interest in permeable flow-control structures, three limitations remain in the existing literature. First, most previous investigations have focused on rigid porous obstacles, permeable collars, baskets, or large woody-debris analogues rather than flexible porous-net systems installed around cylindrical bridge piers. Second, porosity or permeability has generally been evaluated as a geometric property of an obstacle, whereas the role of net density as an adjustable design parameter governing flow penetration and hydraulic resistance has received limited experimental attention. Third, scour-mitigation performance has commonly been evaluated using maximum scour depth alone, which does not fully represent the spatial redistribution of erosion and deposition around the protected pier. The conceptual framework of this study is illustrated in Figure 1.

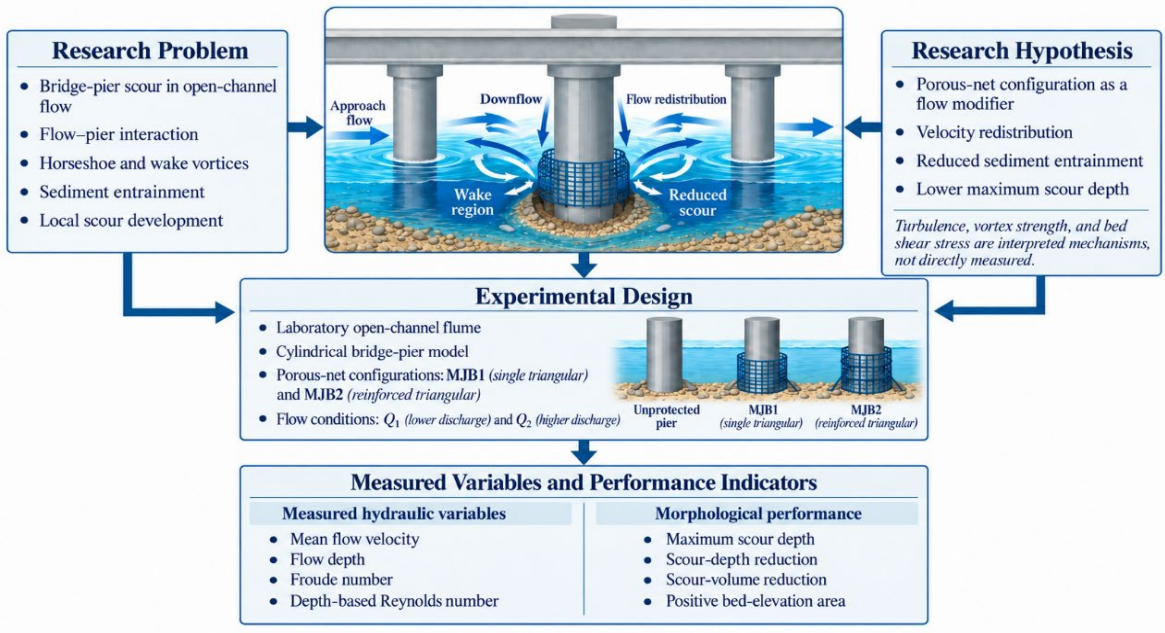


Figure 1. Conceptual framework of hydrodynamic scour mitigation using porous net structures

The porous-net configuration was selected as the principal design parameter because it determines the proportion of the incoming flow that can pass through the structure. A relatively low-density net permits greater flow transmission, whereas a denser or reinforced net provides higher hydraulic resistance and greater momentum attenuation. These differences are expected to influence near-pier velocity and the capacity of the flow to entrain and redistribute bed sediment. Thus, evaluating net density provides a direct basis for linking an adjustable structural characteristic of the protection system to its hydraulic and morphological performance. In this study, vortex attenuation and bed-shear-stress reduction are treated as physically supported interpretations of the measured flow and bed responses rather than directly measured quantities.

Accordingly, this study experimentally compares an unprotected cylindrical pier with two porous-net configurations representing different relative densities and structural arrangements under two discharge conditions. The objectives are to: (1) determine how porous-net configuration and relative density affect the longitudinal flow characteristics; (2) quantify their effectiveness in reducing maximum local scour depth; and (3) evaluate the broader morphological response using scour volume and area-based bed-elevation change.

The principal contribution of this study is a multi-metric experimental framework that connects an adjustable porous-net design characteristic with both local and spatial indicators of scour mitigation. Unlike approaches based only on maximum scour depth, the proposed assessment integrates maximum depth, total scour volume, and the spatial extent of positive bed-elevation change. This combination provides a more comprehensive understanding of whether a countermeasure merely reduces the deepest point of the scour hole or also limits the overall magnitude and spatial extent of

bed erosion.

The novelty of this study lies in the comparative experimental evaluation of flexible porous-net configurations as adjustable flow-modifying countermeasures and in the integration of three complementary morphological indicators: maximum scour depth, total scour volume, and area-based bed-elevation change. This approach extends previous scour assessments, which were mainly based on a single maximum-depth indicator, and provides a more spatially comprehensive explanation of how porous-net configuration and relative density affect local scour mitigation around cylindrical bridge piers.

2. LITERATURE REVIEW

2.1 Bridge pier scour in open-channel flow

Local scour around bridge piers is widely recognized as a primary cause of bridge foundation instability in river environments. When an approaching flow encounters a bridge pier, the flow structure is significantly modified due to the obstruction introduced by the pier geometry [10]. This interaction between the flow and the pier generates complex hydrodynamic phenomena that strongly influence sediment transport processes.

One of the most important mechanisms associated with bridge pier scour is the formation of downflow at the upstream face of the pier [11]. The approaching flow decelerates near the stagnation point and is redirected downward toward the riverbed. This downward jet accelerates near the bed surface, increasing local bed shear stress and initiating sediment motion and erosion around the base of the pier.

In addition to downflow, the interaction between the incoming flow and the pier generates a horseshoe vortex system around the upstream base of the pier. The horseshoe vortex forms due to boundary-layer separation as the flow encounters the obstruction. This vortex continuously rotates around the pier base and enhances sediment entrainment from the riverbed. Downstream of the pier, wake vortices develop as a result of flow separation behind the structure. These vortices contribute to sediment redistribution and further expansion of the scour hole. The combined effects of downflow, horseshoe vortices, and wake vortices result in progressive scour development around the pier [12].

The magnitude of local scour depends on several hydraulic parameters, including flow velocity, flow depth, sediment characteristics, and pier geometry. Understanding these hydrodynamic mechanisms is therefore essential for developing effective strategies to mitigate scour around bridge piers.

2.2 Hydrodynamic interaction between flow and bridge piers

Flow around bluff bodies, such as bridge piers, has been widely studied in hydraulic engineering due to their complex vortex dynamics and implications for sediment transport [13]. When the incoming flow interacts with a cylindrical pier, it undergoes separation, vortex shedding, and turbulent generation. These hydrodynamic processes are strongly influenced by the Reynolds number (*Re*), which determines whether the flow remains laminar or becomes turbulent. At higher *Re*, vortex shedding becomes more pronounced, leading to stronger turbulent and fluctuating forces around the structure.

The vortex structures generated around cylindrical piers can significantly modify the distribution of turbulent kinetic energy and *Re* shear stress in the surrounding flow field. Such hydrodynamic features play a crucial role in controlling sediment entrainment and scour development. Experimental investigations have shown that modifications to the flow field near bluff bodies can significantly alter vortex dynamics and reduce turbulent intensity [14]. These findings suggest that controlling the flow structures around bridge piers can be an effective strategy for mitigating scour formation.

2.3 Mechanisms of sediment entrainment and local scour development

Sediment entrainment occurs when the hydrodynamic forces acting on bed particles exceed the critical shear stress required to initiate motion. Around bridge piers, the combination of downflow acceleration and vortex circulation significantly increases the bed shear stress near the pier base [15]. The erosion process begins when the local bed shear stress surpasses the critical threshold for sediment movement. Once sediment particles are dislodged, they are transported by the surrounding flow and deposited downstream of the pier, leading to the formation of a scour hole. The development of the scour hole further modifies the local flow field. As the scour depth increases, the vortex system becomes stronger, and the downflow penetrates deeper into the bed [16]. This feedback mechanism accelerates the scour process and can lead to significant erosion around bridge foundations. Because of this self-reinforcing mechanism, controlling the hydrodynamic processes that drive sediment entrainment is crucial for reducing scour.

2.4 Existing scour mitigation methods

Various engineering techniques have been developed to mitigate scour around bridge piers. These countermeasures generally fall into two categories: bed-protection methods and flow-modification methods. Bed protection methods aim to increase the resistance of the riverbed material against erosion [17]. Typical examples include riprap, gabions, concrete blocks, and geotextile mats. While these methods can effectively protect the bed surface, they often require large quantities of construction materials and may become unstable under extreme hydraulic conditions. Flow modification methods aim to reduce the intensity of the hydrodynamic processes responsible for scour formation. These techniques alter the flow field around the pier to weaken vortex formation and reduce bed shear stress. Common flow control devices include collars, splitter plates, guide vanes, submerged vanes, and pier slots. These devices modify the flow pattern around the pier and reduce the strength of the horseshoe vortex system. However, many of these structures are rigid and may require complex installation procedures. Recent research has therefore explored alternative flow control techniques that are simpler and more adaptable to hydraulic environments [18].

2.5 Porous structures as flow control devices

Porous structures have emerged as a promising approach for hydraulic flow control due to their ability to dissipate flow energy while allowing partial fluid penetration [19]. Unlike

solid barriers that completely block flow, porous structures allow a portion of the flow to pass through their openings, reducing stagnation pressure and flow contraction. The presence of a porous medium increases hydraulic resistance and promotes momentum dissipation within the flow [20]. As water passes through the porous structure, part of its kinetic energy is converted into turbulent and frictional losses, reducing the effective flow velocity downstream. This mechanism can significantly weaken vortex formation and reduce turbulent intensity around hydraulic structures. By attenuating the approaching flow energy, porous structures can modify the near-bed velocity distribution and decrease the bed shear stress acting on the sediment bed.

2.6 Influence of porous-net density on flow hydrodynamics

Among various porous flow-control systems, porous nets are a flexible, practical structure that can be installed around bridge piers to modify the surrounding flow field. The density of the porous-net determines the level of flow resistance and energy dissipation generated by the structure [21]. A porous net with a higher density provides greater resistance to incoming flow, leading to stronger velocity reduction and greater turbulence attenuation. Conversely, a lower-density porous-net allows greater flow penetration and may produce weaker hydrodynamic modification. Changes in porous-net density, therefore, influence several key hydraulic parameters, including flow velocity distribution, turbulent intensity, vortex strength around the pier, and bed shear stress near the sediment bed. These hydrodynamic changes directly affect the sediment entrainment process and ultimately determine the magnitude of local scour depth.

Despite growing interest in porous flow-control devices, few studies have systematically examined how varying porous-net densities affect scour reduction around cylindrical bridge piers [22]. Most previous studies have focused primarily on rigid flow-control structures rather than on flexible porous systems. Therefore, further experimental investigations are needed to better understand the hydrodynamic effects of porous-net density on scour development and to evaluate its effectiveness as a scour mitigation strategy.

2.7 Critical comparison of previous studies

Previous studies on bridge-pier scour mitigation have generally examined two approaches: direct bed protection and flow modification. Bed-protection methods, including riprap, gabions, and geotextile systems, increase resistance against sediment erosion but may require substantial construction materials and alter natural sediment-transport processes. Flow-modification devices, including collars, slots, guide vanes, and permeable countermeasures, instead seek to modify the downflow, horseshoe-vortex system, and near-bed hydraulic forcing responsible for scour development.

Permeable countermeasures modify pier-induced scour by allowing partial flow transmission rather than completely obstructing the approaching flow. Permeable collars have been shown to reduce local scour by modifying downflow and horseshoe-vortex development, while porous baskets provide localized protection through combined flow resistance and sediment retention. Their effectiveness depends on the opening ratio, geometric arrangement, and installation position relative to the pier.

Pan et al. [3] demonstrated that permeability modifies bleed flow, wake velocity, turbulent kinetic energy, and erosion–deposition patterns around cylindrical structures. Panici and Kripakaran [23] similarly showed that the porosity of large woody-debris accumulations influences localized scour at bridge piers. More recently, Tang and Li [24] reported that obstacle porosity affects flow partitioning, bed shear stress, and vertical-contraction scour. These findings indicate that permeability and structural density are important parameters that control the interactions among flow resistance, turbulent, and sediment transport. Nevertheless, most existing studies have investigated rigid porous obstacles, permeable collars, porous baskets, or woody-debris analogues. Compared with other countermeasures, relatively limited attention has been given to flexible porous-net countermeasures installed around cylindrical bridge piers. In addition, previous assessments have frequently emphasized maximum scour depth without simultaneously evaluating scour volume and spatial changes in bed elevation.

3. METHODOLOGY

3.1 Hydraulic flume configuration

The main geometric and hydraulic parameters of the laboratory flume used in this study are summarized in Table 1. These parameters define the experimental conditions for investigating the hydrodynamic interaction between the approaching flow and the cylindrical bridge pier with porous net protection.

Table 1. Hydraulic flume and experimental parameters

Parameter	Symbol	Value	Unit	Description
Flume length	L	12.0	m	Total length of the experimental channel
Flume width	B	0.60	m	Internal width of the rectangular flume
Flume height	Hf	0.50	m	Total height of the flume wall
Flow depth	h	0.15	m	Water depth during experiments
Pier diameter	D	0.05	m	Diameter of the cylindrical bridge pier
Sediment median size	d_{50}	0.80	mm	Median diameter of bed material
Sediment density	ρ_s	2650	kg/m³	Density of sediment particles
Water density	ρ	1000	kg/m³	Density of water
Kinematic viscosity	ν	8.69×10^{-7} m²/s	m²/s	Kinematic viscosity of water
Gravitational acceleration	g	9.81	m/s²	Gravitational acceleration
Discharge condition 1	Q_1	1.33×10^{-4}	m³/s	Low discharge condition
Discharge condition 2	Q_2	2.10×10^{-4} m³/s	m³/s	High discharge condition

3.2 Porous-net configurations and installation

Two porous-net countermeasures were evaluated in the experiments. Both were constructed using commercially available flexible polymer netting supported by a rigid wire frame and installed upstream of the cylindrical pier. MJB1 consisted of a single triangular net arrangement, whereas MJB2 employed a reinforced triangular arrangement incorporating additional overlapping net elements. Therefore, the configurations differed primarily in their structural arrangement and effective flow blockage rather than in independently calibrated material porosity.

Based on the nominal model dimensions and available experimental documentation, both configurations had an approximate length of 20 cm, width of 20 cm, and height of 10 cm, corresponding to 4D × 4D × 2D, where the pier diameter D was 5 cm. The net had an approximately square mesh opening of 5 × 5 mm. The upstream boundary of the structure was positioned approximately 5 cm ($1D$) from the upstream face of the pier. Its lower edge was placed flush with the initial sediment-bed surface, and the structure was aligned symmetrically with the longitudinal centreline of the pier. The external dimensions and installation arrangement were maintained consistently for both configurations.

MJB2 provided greater flow obstruction than MJB1 because of its reinforced arrangement. Since porosity and solidity were not directly measured, the results represent a comparison of net configurations rather than a calibrated density–scour relationship.

3.3 Hydraulic flow conditions

The experiments were conducted under controlled discharge conditions representing different levels of hydraulic forcing in the open-channel flume. The hydraulic conditions were characterized using mean flow velocity V, flow depth h, depth-based Reynolds number (Re_h), and Froude number (Fr). These dimensionless parameters describe the relative influence of viscous and gravitational forces and provide a consistent basis for comparing the flow conditions associated with the MJB1 and MJB2 configurations [25, 26].

The depth-based *Re* was calculated as:

$$Re_h = \frac{Vh}{\nu} \tag{1}$$

where, V is the mean flow velocity (m/s), h is the local flow depth (m), and ν is the kinematic viscosity of water (m^2/s). The parameter Re_h represents the ratio of inertial to viscous effects based on the measured flow depth.

The *Fr* was calculated as:

$$Fr = \frac{V}{\sqrt{gh}} \tag{2}$$

where, g is gravitational acceleration (9.81 m/s²). The Fr represents the ratio of inertial to gravitational effects and was used to classify the local flow as subcritical ($Fr < 1$), critical ($Fr = 1$), or supercritical ($Fr > 1$). The calculated Re_h and Fr values characterize the hydraulic regime at the measurement stations. They do not directly quantify turbulent intensity, vortex strength, or bed shear stress; these processes require direct spatial flow measurements.

3.4 Scour depth measurement

The development of local scour around the bridge pier was monitored during each experimental run. After the flow conditions reached equilibrium, the bed surface elevation was measured along the longitudinal centerline passing through the pier [27]. This measurement allowed the identification of the scour-hole geometry and the determination of the maximum scour depth. The maximum scour depth was obtained by comparing the final bed elevation after the experiment with the initial bed level prior to the flow test. The scour depth is defined as:

$$d_s = z_0 - z_f \tag{3}$$

where, d_s is the local scour depth (m), z_0 is the initial bed elevation before the experiment (m), and z_f is the final bed elevation after the experiment (m). The parameter d_s represents the vertical difference between the initial sediment-bed elevation and the lowest bed elevation measured around the pier after the experiment.

3.5 Scour-mitigation performance indicators

Three complementary indicators were used to evaluate scour mitigation: maximum scour-depth reduction, scour-volume reduction, and area-based bed recovery. All calculations used the same measured bed domain and the unprotected pier under the corresponding discharge condition as the reference. Bed-elevation change at each measurement cell was defined as:

$$\Delta z_i = z_{f,i} - z_{0,i} \tag{4}$$

where, $z_{0,i}$ and $z_{f,i}$ are the initial and final bed elevations at cell i, respectively. Thus, $\Delta z_i < 0$ indicates erosion, whereas $\Delta z_i > 0$ indicates deposition or positive bed-elevation change.

Maximum scour depth represents the greatest vertical erosion observed within the measurement domain:

$$d_{s,max} = \max_i \left(z_{0,i} - z_{f,i}\right)$$

Its reduction relative to the unprotected pier was calculated as:

$$R_d = \frac{d_{s,0} - d_{s,p}}{d_{s,0}} \times 100\% \tag{5}$$

where, $d_{s,0}$ and $d_{s,p}$ are the maximum scour depths for the unprotected and protected conditions, respectively.

Scour volume represents the cumulative negative bed-elevation change over the evaluated area:

$$V_s = \sum_{i=1}^{n} max\,(0, -\Delta z_i)\Delta A_i \tag{6}$$

where, ΔA_i is the area represented by measurement cell i. Scour-volume reduction was determined as:

$$R_V = \frac{V_{s,0} - V_{s,p}}{V_{s,0}} \times 100\% \tag{7}$$

This indicator measures the reduction in total sediment deficit and differs physically from maximum scour-depth reduction, which represents only the deepest erosion point.

The area-based bed recovery ratio was defined as the proportion of the measured domain exhibiting positive bed-elevation change:

$$R_A = \frac{\sum_{i=1}^{n} I\,(\Delta z_i > 0)\Delta A_i}{\sum_{i=1}^{n} \Delta\, A_i} \times 100\% \qquad (8)$$

where, $I(\cdot)$ equals 1 when the condition is satisfied and 0 otherwise. This indicator describes the spatial extent of deposition or positive elevation change and does not represent the percentage of eroded sediment volume that was restored.

4. RESULT AND DISCUSSION

4.1 Hydraulic flow characteristics around the cylindrical pier

The hydraulic behavior of the approaching flow around the cylindrical bridge pier was evaluated using the *Fr* and *Re*, which are key indicators of the flow regime and turbulent characteristics governing sediment entrainment and scour formation. Flow approaching a bridge pier undergoes strong hydrodynamic disturbance characterized by flow deceleration at the stagnation zone, downward impinging flow (downflow), development of horseshoe vortices around the pier base, and wake vortices downstream of the pier.

These vortex systems increase near-bed shear stress and mobilize sediment particles, ultimately forming a scour hole around the pier foundation. The present study investigates how porous-net with different densities modify these hydrodynamic processes and reduce scour depth. Hydraulic measurements were conducted at 12 longitudinal stations downstream of the pier. The measured variables include flow velocity, flow depth, *Re*, and *Fr*.

4.2 Froude number distribution

The interactions between flow resistance and turbule configurations under the higher tested discharge condition (Q_2) are summarized in Table 2. The flow regime was classified as subcritical for $Fr < 1$, critical for $Fr = 1$, and supercritical for $Fr > 1$.

Table 2. Froude number (*Fr*) distribution along the channel

Station	*Fr* (MJB1)	Flow Regime	*Fr* (MJB2)	Flow Regime
S1	1.091	Supercritical	1.328	Supercritical
S2	1.117	Supercritical	1.298	Supercritical
S3	1.141	Supercritical	1.269	Supercritical
S4	1.061	Supercritical	1.106	Supercritical
S5	1.034	Supercritical	1.088	Supercritical
S6	1.071	Supercritical	1.039	Supercritical
S7	1.088	Supercritical	1.039	Supercritical
S8	0.946	Subcritical	0.974	Subcritical
S9	0.808	Subcritical	0.723	Subcritical
S10	0.850	Subcritical	0.702	Subcritical
S11	0.746	Subcritical	0.629	Subcritical
S12	0.793	Subcritical	0.652	Subcritical

As shown in Table 2, both configurations exhibited supercritical flow at upstream stations S1–S7 and subcritical flow at downstream stations S8-S12. The transition occurred between S7 and S8, where the *Fr* decreased from above to below unity. MJB2 produced higher *Fr* than MJB1 at S1-S5, whereas the opposite pattern was generally observed farther downstream. These results indicate that the reinforced porous-net configuration redistributed the local hydraulic conditions along the measurement section rather than uniformly reducing the *Fr*.

Figure 2 presents the longitudinal distribution of mean flow velocity at measurement stations S1–S12 for the MJB1 and MJB2 configurations under the higher tested discharge condition (Q_2). Both configurations show relatively high velocities at the upstream stations, followed by an overall decrease toward the downstream stations. Differences between the two profiles indicate that the reinforced arrangement of MJB2 modified the longitudinal distribution of flow velocity rather than producing a uniform reduction along the entire measurement section. This redistribution of flow momentum may have contributed to the lower scour depth observed for MJB2. However, because turbulent intensity and vortex strength were not measured directly, their modification is interpreted as a physically plausible mechanism rather than a directly verified process.

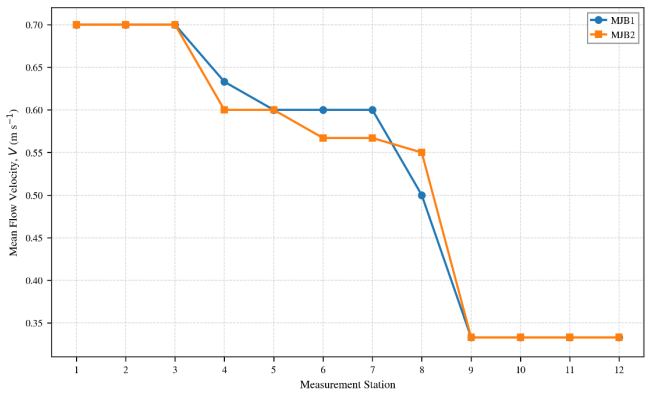


Figure 2. Longitudinal distribution of mean flow velocity (*m/s*) at measurement stations S1-S12 for the MJB1 and MJB2 porous-net configurations under the higher tested discharge condition (Q_2)

4.3 Reynolds number analysis

The depth-based *Re* calculated for the MJB1 and MJB2 configurations under the higher tested discharge condition (Q_2) is presented in Table 3. The flow regime was classified as laminar for $Re_h < 2000$, transitional for $2000 \leq Re_h \leq 4000$, and turbulent for $Re_h > 4000$. Furthermore, the *Re* distribution is illustrated in Figure 3.

For MJB1, the tabulated *Re* were 33,833.5; 32,222.4; 30,879.8; 26,481.2; 23,706.5; 22,095.4; 21,404.9; 16,398.9; 6,649.1; 6,009.7; 7,799.9 and 6,904.8 from Stations 1 to 12. The kinematic viscosity was adjusted based on the measured water temperature during the experiment. At Station 1, MJB1, Q_2, the table gives:

- $V = 0.700$ m/s
- $H = 0.042$ m
- $\nu = 8.69 \times 10^{-7}$ m²/s (at T ≈ 26.8 °C)
- $Re_h = \frac{0.700 \times 0.042}{0.000000869} = \frac{0.0294}{8.69 \times 10^{-7}} = 33{,}833.5$

As shown in Table 3, all measurement stations exhibited turbulent flow under Q_2, with Re_h ranging from 6,009.7 to

33,833.5 for MJB1 and from 8,311.3 to 24,972.4 for MJB2. In both configurations, the *Re* generally decreased from upstream to downstream stations, though local variations occurred, particularly in MJB2. The lower downstream values indicate a reduction in the relative influence of inertial forces along the measurement section. However, they remained above the adopted turbulent-flow threshold.

Table 3. Distribution of the depth-based Reynolds number (*Re*) under Q_2

Station	Re_h(MJB1)	Flow Regime	Re_h(MJB2)	Flow Regime
S1	33,833.5	Turbulent	22,824.2	Turbulent
S2	32,222.4	Turbulent	23,898.3	Turbulent
S3	30,879.8	Turbulent	24,972.4	Turbulent
S4	26,481.2	Turbulent	20,714.4	Turbulent
S5	23,706.5	Turbulent	21,404.9	Turbulent
S6	22,095.4	Turbulent	19,781.0	Turbulent
S7	21,404.9	Turbulent	19,781.0	Turbulent
S8	16,398.9	Turbulent	20,570.6	Turbulent
S9	6,649.1	Turbulent	8,311.3	Turbulent
S10	6,009.7	Turbulent	8,822.8	Turbulent
S11	7,799.9	Turbulent	10,996.5	Turbulent
S12	6,904.8	Turbulent	10,229.3	Turbulent

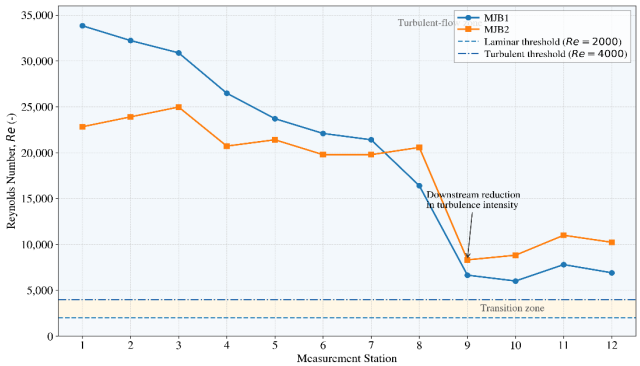


Figure 3. Longitudinal distribution of the depth-based Reynolds number (*Re*) at measurement stations S1-S12 for MJB1 and MJB2 under Q_2

Note: The horizontal dashed lines indicate the adopted laminar (Re_h = 2000) and turbulent (Re_h = 4000) thresholds. All measured values are within the turbulent-flow regime.

4.4 Froude number distribution and hydraulic interpretation

The velocity profile shows a gradual decrease downstream due to energy dissipation, turbulent generation, and flow obstruction by the pier and the porous-net. The presence of the porous-net reduces near-bed velocity and redistributes the incoming flow momentum. The *Fr* distributions indicate that both configurations exhibited supercritical flow at stations S1–S7 and subcritical flow at stations S8–S12, with the transition occurring between S7 and S8. MJB2 produced higher *Fr* than MJB1 at S1–S5, whereas MJB1 generally produced higher values farther downstream. These patterns indicate that MJB2 redistributed the local hydraulic conditions along the measurement section rather than uniformly reducing the *Fr*. Figure 4 presents the longitudinal *Fr* distributions for MJB1 and MJB2 under Q_2.

The reduction in scour depth can be attributed to the disruption of coherent vortex structures. The porous-net introduces distributed resistance, dissipating kinetic energy and weakening the strength of horseshoe vortices. As a result, the near-bed shear stress decreases, limiting sediment entrainment capacity.

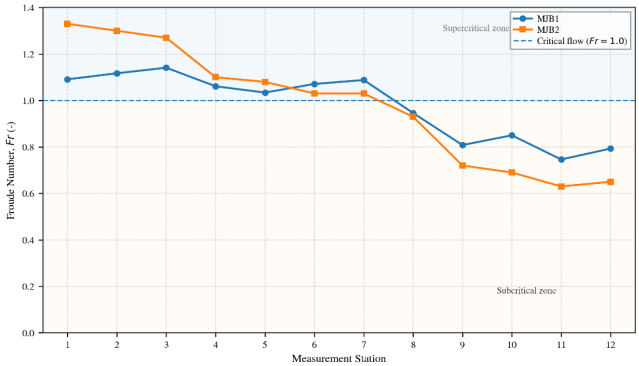


Figure 4. Longitudinal distribution of the Froude number (*Fr*) at measurement stations S1-S12 for MJB1 and MJB2 under Q_2

4.5 Maximum scour depth

The maximum scour depths obtained during the experiments are summarized in Table 4.

The maximum scour-depth reduction of 83.36% was obtained for MJB2 under the higher tested discharge condition (Q_2). Under this condition, MJB2 reduced the maximum scour depth from approximately 5.4 cm for the unprotected pier to 0.9 cm. The experiment was conducted at the laboratory scale using a 0.05-m-diameter cylindrical pier, a flow depth of 0.15 m, and uniform sediment with d_{50} = 0.80 mm and ρ_s = 2650 kg·m^{-3}. Consequently, the reported reduction reflects MJB2's relative performance under the investigated hydraulic, sediment, and geometric conditions and should not be interpreted as a universally applicable scour-reduction efficiency. Furthermore, all results of the calculation are visualized in Figure 5.

Table 4. Scour depth under Q_1 and Q_2

Model	Scour Depth Under Q_1		Scour Depth Under Q_2	
	Depth (cm)	Reduction (%)	Depth (cm)	Reduction (%)
MJB1	2.5	44.4	1.5	77.27
MJB2	1.4	68.9	0.9	83.36

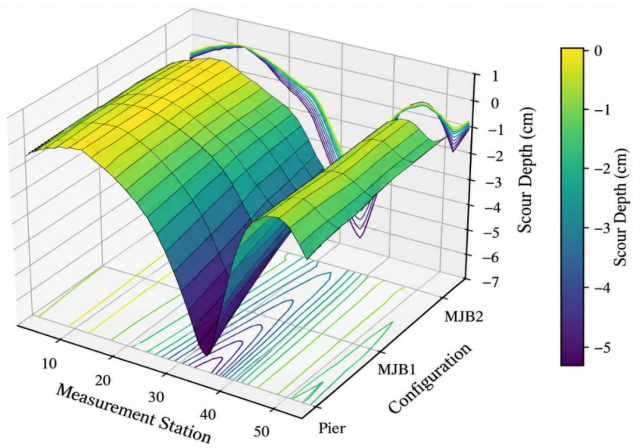


Figure 5. Longitudinal scour-depth profiles (cm) for the unprotected pier, MJB1, and MJB2 under Q_2

Based on the results in Table 4, the following is a calculation example, using the Q_1-MJB1 data:

$$44.4 = \frac{d_{s,0,Q_1} - 2.5}{d_{s,0,Q_1}} \times 100$$
$$d_{s,0,Q_1} = 4.5\ cm$$

Using the same baseline depth for MJB2:

$$R_s = \frac{4.5 - 1.4}{4.5} \times 100; = 68.9\%$$

The results demonstrate that porous-net provides an effective passive scour-protection mechanism around cylindrical bridge piers. Compared with traditional countermeasures such as riprap or collars, porous-net offers several advantages: reduced construction cost, flexible installation, effective turbulence attenuation, and significant scour-depth reduction (up to 83.36%). These findings indicate that porous-net could serve as a practical hydraulic control technique for bridge scour mitigation in river engineering applications.

4.6 Bed elevation difference analysis

To further quantify the spatial redistribution of sediment, the bed elevation difference between the initial and post-test conditions was analyzed. This approach provides insight into both erosion and deposition patterns, enabling a more comprehensive assessment of morphological changes beyond localized scour depths.

Under baseline conditions, the bed elevation difference map shows a pronounced erosion zone concentrated at the upstream face of the pier, extending laterally due to the influence of the horseshoe vortex system. The maximum negative elevation values indicate intense sediment removal driven by strong downflow and accelerated near-bed velocities. Downstream of the pier, deposition zones are observed, corresponding to sediment transport and re-settling within the wake region. With the installation of porous-net, a significant modification of the bed morphology is observed. The erosion zone becomes less intense and more spatially confined, while deposition patterns are more evenly distributed. This indicates that the porous structure effectively reduces the energy available for sediment entrainment and promotes more stable sediment redistribution. The result is visualized in Figure 6.

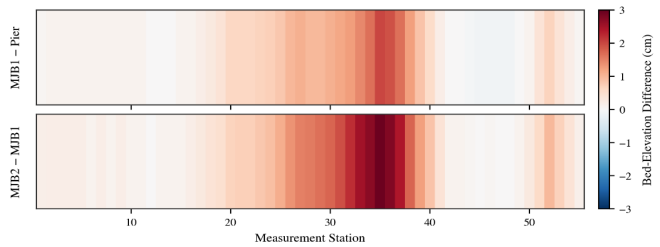


Figure 6. Bed-elevation difference maps under Q_2 with MJB1 relative to the unprotected pier and MJB2 relative to the unprotected pier

The stronger morphological response of MJB2 can be related to its higher relative structural density and greater effective flow blockage. Its additional net elements divide the approaching flow into transmitted, lateral, and overtopping components, thereby redistributing momentum before the flow reaches the pier. This redistribution may reduce the concentration of near-bed forcing at the upstream pier base, where downflow and the horseshoe vortex system commonly initiate sediment entrainment. The smaller negative bed-elevation region and broader positive elevation pattern observed for MJB2 are therefore consistent with reduced sediment removal and increased retention or redeposition within the protected region. However, because vorticity and bed shear stress were not directly measured, these processes are interpreted as physically plausible mechanisms rather than directly verified quantities.

4.7 Quantitative scour volume reduction analysis

To further quantify the effectiveness of porous-net configurations, the total scour volume was evaluated by integrating the bed elevation difference along the measurement section.

The results clearly demonstrate that porous-net installation reduced scour volume under the investigated conditions, with the highest-density configuration (MJB2) achieving a 43.7% reduction. This indicates that enhanced flow resistance and the observed response are consistent with reduced sediment-entrainment forcing, thereby limiting scour development. The results indicate that both porous-net configurations significantly reduce the total scour volume compared to the unprotected pier. The reinforced triangular configuration demonstrates the highest reduction, confirming its superior ability to dissipate flow energy and redistribute sediment transport. This volumetric analysis provides a more comprehensive metric than maximum scour depth alone, as it captures the overall morphological impact of scour mitigation measures across the entire interaction zone. The computed scour volume reduction for each configuration is presented in Figure 7.

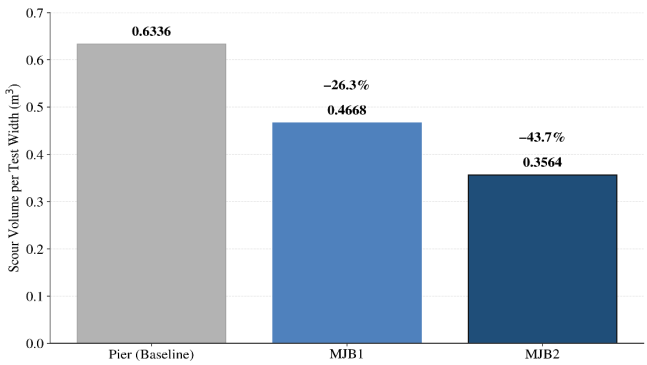


Figure 7. Total scour volume for the unprotected pier, MJB1, and MJB2 under Q_2

The volumetric reduction supports the bed-elevation analysis by demonstrating that MJB2 reduced the overall sediment deficit rather than merely shifting the deepest scour location. Its reinforced porous arrangement provides distributed hydraulic resistance while retaining partial flow permeability. This combination may reduce the concentration of momentum near the pier without causing the abrupt flow separation associated with an impermeable barrier. Consequently, sediment-entrainment capacity is reduced in the protected region, while a larger proportion of mobilized sediment is retained or redeposited nearby. The agreement among lower maximum scour depth, reduced scour volume,

and broader positive bed-elevation change provides complementary evidence of MJB2's superior mitigation performance.

4.8 Area-based bed recovery assessment

In addition to volumetric reduction, the spatial extent of bed recovery was evaluated using the percentage of positive elevation difference relative to the total measured area.

The results indicate that increasing porous net density significantly enhances bed recovery performance. The MJB2 configuration achieved an area recovery of 98.2%, approaching full restoration of the bed surface, confirming its effectiveness in attenuating near-bed flow energy and limiting sediment mobilization. The reinforced porous-net configuration exhibits the largest recovery area, indicating a more effective stabilization of the riverbed. The distribution of positive elevation zones confirms that sediment deposition is not limited to localized regions but extends across a broader area surrounding the pier. This metric highlights porous structures' ability to promote sediment retention and reduce erosion susceptibility across a wider spatial domain. The results are illustrated in Figure 8.

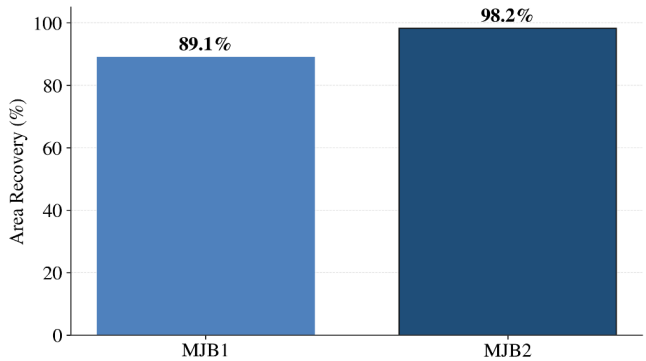


Figure 8. Percentage of the evaluated bed area exhibiting positive elevation change for MJB1 and MJB2 relative to the unprotected-pier condition under Q_2

4.9 Relative shear-stress interpretation

The critical shear stress of the bed material, τ_c. Sediment motion is initiated when:

$$\tau_b > \tau_c$$

Under comparable bed conditions, the applied shear stress can be conceptually related to the local velocity such as:

$$\tau_b = C_f \rho V^2$$

where, C_f is the bed-friction coefficient, ρ is the water density, and V is the local flow velocity. This relationship indicates that changes in velocity distribution can produce proportionally larger changes in the hydrodynamic force acting on the sediment bed.

The porous-net configurations did not generate a uniform reduction in hydraulic intensity along the channel. Instead, they redistributed the approaching flow among the transmitted, lateral, and overtopping components. The higher relative structural density of MJB2 increased effective flow obstruction and modified the spatial distribution of momentum around the pier. This redistribution may have reduced the concentration of near-bed hydraulic forcing at the upstream pier base, where downflow and the horseshoe-vortex system commonly generate the highest sediment capacity.

The morphological results support this interpretation. MJB2 reduced maximum scour depth by 68.9% under Q_1 and 83.36% under Q_2, decreased total scour volume by 43.7%, and produced the largest area of positive bed-elevation change. The simultaneous reduction in maximum scour depth and total scour volume indicates that MJB2 limited both localized erosion and the overall sediment removal from the measured region. These responses are consistent with reduced or spatially redistributed bed-shear forcing. However, τ_b, vorticity, turbulent kinetic energy, and *Re* shear stress were not directly measured. Therefore, the proposed reduction and redistribution of bed shear stress should be interpreted as a physically supported explanation based on the measured hydraulic and morphological responses, rather than as direct experimental verification. Future studies using particle image velocimetry, acoustic Doppler velocimetry, or validated three-dimensional numerical modelling are required to quantify these mechanisms directly.

4.10 Comparison with previous studies

Compared to conventional scour countermeasures such as collars and riprap, which primarily act as passive protective systems, the porous-net approach operates through active flow modification. This distinction highlights a shift from structural resistance to hydrodynamic control as the governing mitigation strategy. The present results therefore contribute to an emerging paradigm in scour mitigation, in which turbulent regulation and vortex suppression are prioritized over bed armoring. To strengthen the interpretation of the results, this study compared its findings with several previous studies that examined the use of porous or permeable structures for erosion mitigation, as presented in Table 5.

Previous research has shown that porous structures can modify the flow rate distribution and reduce turbulent intensity around the structure. This condition causes a decrease in the base shear stress, thereby reducing the flow's ability to transport sediment. Our findings are consistent with the results of this study's experiment, which showed that the porous mesh significantly reduced the scour depth. The results indicate that the porous-net configuration influences hydraulic and morphological responses near the pier rather than bulk-flow energy. The suppression of coherent vortex systems reduces localized shear stress concentration at the pier base, the dominant mechanism controlling sediment entrainment. This indicates that scour mitigation is achieved through targeted hydrodynamic regulation rather than global flow reduction.

The applicability of the findings is limited to the investigated laboratory conditions: steady flow, a rectangular flume, a cylindrical pier with $D = 0.05$ m, a constant flow depth of 0.15 m, uniform sediment with $d_{50} = 0.80$ mm, and the tested discharge and porous-net configurations. The results demonstrate the relative performance of MJB1 and MJB2 within this experimental domain but should not be interpreted as universal design values. Application to field-scale bridge piers requires consideration of hydraulic similarity, sediment gradation, flow unsteadiness, pier geometry, debris loading, net deformation, and long-term structural durability.

The reinforced MJB2 configuration demonstrated effective scour mitigation under the investigated laboratory conditions;

however, its field implementation would require further engineering evaluation. The system would need a stable anchorage arrangement capable of resisting drag, uplift, deformation, and cyclic loading without destabilizing the surrounding bed. Net durability may also be affected by abrasion, ultraviolet exposure, corrosion of supporting components, and repeated hydraulic loading. Floating debris, vegetation, and sediment could obstruct the mesh openings, alter the effective porosity, increase hydraulic forces, and reduce the intended flow-transmission performance. Therefore, periodic inspection, debris removal, and component replacement may be necessary. The present results establish the hydraulic potential of the porous-net concept but do not demonstrate its long-term durability or field-scale reliability. Further testing under unsteady flood flows, debris loading, heterogeneous sediments, and prolonged exposure is required before the system can be recommended for practical bridge-pier protection.

Table 5. Comparison with previous studies on scour mitigation using porous structures

Study	Pier/Structure Dimensions	Sediment Condition	Porous Structure Characteristics	Hydraulic Condition	Main Quantitative Result
[3]	Emergent cylindrical structure; D = 0.10 m	Uniform sand; d = 1.0 mm	Surface void ratio, P = 0, 0.38, and 0.62	Q = 0.038 m³/s; h = 0.14 m; V = 0.272 m/s; Fr = 0.23; Re = 38,000	Increasing P from 0.38 to 0.62 reduced wake-velocity attenuation by 38% and decreased side bed shear stress; equilibrium maximum scour-depth reduction was not reported
[7]	Cylindrical pier with permeable collar; collar diameter, thickness, and installation height varied relative to D	Clear-water scour; sediment incipient velocity = 0.349 m/s; d_{50} should be taken from the full paper	Permeable collar; optimum porosity P = 50%; optimum thickness T/D = 0.15	h = 0.20 m; other hydraulic parameters should be taken from the full paper	Maximum scour-depth reduction of 78.1% at P = 50%; reduction reached 89.6% for the optimum collar thickness
[27]	Surface-piercing square monopile; attack angle α = 00–600	Live-bed sediment; d_{50} not reported in accessible metadata	Square porous monopile; P = 0 – 38.8%; streamwise and transverse porosity investigated	Steady current; Q, h, V, and Frnot reported in accessible metadata	Increasing streamwise porosity reduced the equilibrium scour depth by weakening the upstream horseshoe vortex; an exact percentage reduction was not reported in the abstract
This study	Cylindrical pier, D = 0.05 m; MJB1 and MJB2 dimensions 0.20 × 0.20 × 0.10 m	Uniform sediment; d_{50} = 0.80 mm; ρ_s = 2650 kg/m³	Flexible polymer net; nominal mesh opening 5 × 5mm; MJB1: single triangular configuration; MJB2: reinforced triangular configuration.	h = 0.15 m; two steady-flow conditions, Q_1 and Q_2	MJB1 reduced maximum scour depth by 44.4% under Q_1 and 77.27% under Q_2; MJB2 achieved reductions of 68.9% and 83.36%, respectively

5. CONCLUSION

This study experimentally evaluated the effects of relative porous-net density on local scour around a cylindrical bridge pier under two steady-flow conditions. Both configurations reduced the maximum scour depth relative to the corresponding unprotected pier. The reinforced MJB2 configuration achieved reductions of 68.9% under Q_1 and 83.36% under Q_2 . The maximum reduction under Q_2 corresponded to a decrease in scour depth from 5.4 cm for the unprotected pier to 0.9 cm for MJB2. It also reduced the total scour volume by 43.7% and produced the largest area of positive bed-elevation change. Collectively, these indicators show that MJB2 limited both localized scour and the overall sediment deficit within the evaluated bed area.

The improved performance of MJB2 is associated with its higher relative structural density and greater effective flow obstruction. Its reinforced arrangement redistributed the approaching flow and may have reduced the concentration of near-bed hydraulic forcing at the pier base, thereby limiting sediment entrainment and promoting sediment retention or redeposition. However, vortex strength, turbulent intensity, and bed shear stress were not measured directly. Consequently, vortex modification and shear-stress redistribution should be interpreted as physically plausible mechanisms supported by the observed velocity and morphological responses rather than as directly verified processes.

The maximum reduction of 83.36% was obtained specifically under the higher tested discharge condition (Q_2) in a laboratory flume using uniform sediment with $d_{50} = 0.80$ mm and particle density $\rho_s = 2650$ kg m^{-3}, a cylindrical pier with $D = 0.05$ m, and a flow depth of 0.15 m. Therefore, the reported reduction reflects MJB2's relative performance under the investigated hydraulic, sediment, and geometric conditions and should not be interpreted as a universal design efficiency or directly extrapolated to field-scale bridge piers. Further research should evaluate the system under unsteady flood flows, heterogeneous sediments, different pier geometries, debris accumulation, net deformation, anchorage instability, material degradation, and prolonged hydraulic loading. Direct flow-field measurements and validated three-dimensional numerical modelling are also needed before the porous-net system can be recommended for practical field implementation.

ACKNOWLEDGMENT

The authors would like to thank the Management of the Engineering Faculty of Universitas Muhammadiyah Makassar.

REFERENCES

[1] Magrini, Harlan, D., Rasyid, I., Nugroho, J., Adityawan, M.B., Natakusumah, D.K. (2024). Modelling of flow and scour around the piers with different geometric shapes. International Journal of GEOMATE, 26(113): 115-122. https://doi.org/10.21660/2024.113.g13375

[2] Xu, C., Huang, Z. (2023). A laboratory study of wave-induced local scour at an emergent pile breakwater. Ocean Engineering, 270: 113618. https://doi.org/10.1016/j.oceaneng.2023.113618

[3] Pan, J., He, Z., Shih, W., Cheng, N. (2020). Numerical modeling of scour and deposition around permeable cylindrical structures. International Journal of Sediment Research, 35(3): 278-286. https://doi.org/10.1016/j.ijsrc.2020.01.001

[4] Zhang, Q., Tang, G., Lu, L., Yang, F. (2021). Scour protections of collar around a monopile foundation in steady current. Applied Ocean Research, 112: 102718. https://doi.org/10.1016/j.apor.2021.102718

[5] Heravi, Z., Moghaddam, M.A., Esmaili, K., Givehchi, M., Bahrpeyma, A. (2024). Impact of installing new scour prevention countermeasure (F-jacks) around bridge pier on flow pattern and scour control. Ocean Engineering, 313: 119326. https://doi.org/10.1016/j.oceaneng.2024.119326

[6] Nakai, M., Nakabayashi, T., Nishimura, N., Watanabe, K., Yatabe, H. (2023). Porous Plate method: reduction in local scour around pier-type structures in multidirectional flows. Journal of Waterway, Port, Coastal, and Ocean Engineering, 149(2): 06023001. https://doi.org/10.1061/JWPED5.WWENG-1956

[7] Qi, H., Yuan, T., Zhao, F., et al. (2023). Local scour reduction around cylindrical piers using permeable collars in clear water. Water, 15(5): 897. https://doi.org/10.3390/w15050897

[8] Bharadwaj, M.R., Gupta, L.K., Pandey, M. (2024). Reduction of local scour around a circular bridge pier using the collars and sacrificial piles in non-uniform sediment. Geomorphology, 465: 109378. https://doi.org/10.1016/j.geomorph.2024.109378

[9] AsadUllah, M., Ejaz, N., Abbas, G., et al. (2025). Impact of a submerged trapezoidal broad-crested weir on local scouring at a bridge pier under clear water conditions. Engineering Research Express, 7(2): 025102. https://doi.org/10.1088/2631-8695/adc4bf

[10] Gao, P., Mou, X., Ji, H. (2023). Refined simulation study on the effect of scour environments on local scour of tandem bridge piers. Sustainability, 15(9): 7171. https://doi.org/10.3390/su15097171

[11] Hurtado-Herrera, M., Zhang, W., Hammouti, A., Pham Van Bang, D., Nguyen, K.D. (2023). Numerical study of the flow and blockage ratio of cylindrical pier local scour. Applied Sciences, 13(20): 11501. https://doi.org/10.3390/app132011501

[12] Daneshfaraz, R., Ghaderi, A., Sattariyan, M., et al. (2021). Investigation of local scouring around hydrodynamic and circular pile groups under the influence of river material harvesting pits. Water, 13(16): 2192. https://doi.org/10.3390/w13162192

[13] Keshavarz, A., Vaghefi, M., Ahmadi, G. (2021). Investigation of flow pattern around rectangular and oblong piers with collar located in a 180° sharp bend. Scientia Iranica, 28(5): 2479-2492. https://doi.org/10.24200/sci.2021.55320.4169

[14] Qasim, R.M., Faisal, S.H., Jabbar, T.A. (2022). Impact of T-splitter on the laminar flow field around cylinder pier. Advances in Science and Technology Research Journal, 16(5): 202-215. https://doi.org/10.12913/22998624/154795

[15] Muhawenimana, V., Foad, N., Ouro, P., Wilson, C.A.M.E. (2022). Local scour patterns around a bridge pier with cable-wrapping. Fluids, 8(1): 3. https://doi.org/10.3390/fluids8010003

[16] Gao, P., Mou, X., Ji, H. (2023). Simulation study on local scour characteristics of tandem bridge piers in a straight river under a changing environment. Sustainability, 15(15): 11776. https://doi.org/10.3390/su151511776

[17] Fathi, A., Zomorodian, S.A., Zolghadr, M., et al. (2023). Combination of riprap and submerged vane as an abutment scour countermeasure. Fluids, 8(2): 41. https://doi.org/10.3390/fluids8020041

[18] Luo, K., Si, Y., Lu, S., Liang, B., Qi, H. (2022). Characteristics of reducing local scour around cylindrical pier using a horn-shaped collar. Journal of Engineering and Applied Science, 69(1): 105. https://doi.org/10.1186/s44147-022-00160-x

[19] Williams, P., Balachandar, R., Roussinova, V., Barron, R. (2022). Particle image velocimetry evaluation of flow-altering countermeasures for local scour around a submerged circular cylinder. International Journal of Sediment Research, 37(4): 411-423. https://doi.org/10.1016/j.ijsrc.2022.03.001

[20] Yang, F., Qu, L., Tang, G., Lu, L. (2021). Local scour around a porous surface-piercing square monopile in steady current. Ocean Engineering, 223: 108716. https://doi.org/10.1016/j.oceaneng.2021.108716

[21] Zhang, Y., Wang, J., Zhou, Q., Cai, Y., Tang, W. (2023). The investigation of local scour around bridge piers with the protection of a quasi-stumps group. Water, 15(15). https://doi.org/10.3390/w15152858

[22] Lee, W.L., Lu, C.W., Huang, C.K. (2021). Application of a single porous basket as a pier scour countermeasure. Water, 13(21): 3052. https://doi.org/10.3390/w13213052

[23] Panici, D., Kripakaran, P. (2023). Characterizing the importance of porosity of large woody debris accumulations at single bridge piers on localized scour. Water Resources Research, 59(9): e2022WR033531. https://doi.org/10.1029/2022WR033531

[24] Tang, Z., Li, Y.P. (2026). Vertical contraction scour beneath solid and porous obstacles in steady currents: A numerical and theoretical study. Coastal Engineering, 205: 104936. https://doi.org/10.1016/j.coastaleng.2025.104936

[25] Harasti, A., Gilja, G., Potočki, K., Lacko, M. (2021). Scour at bridge piers protected by the riprap sloping structure: A review. Water, 13(24): 3606. https://doi.org/10.3390/w13243606

[26] Abdulwahd, A.K., Maatooq, J.S. (2023). Experimental investigation of local scour under two oblong piers of a bridge crossing a sharp bend river. Journal of Water and

Land Development, 58: 129-135. https://doi.org/10.24425/jwld.2023.146605
[27] Yang, F., Qu, L., Zhang, Q., Tang, G., Liang, B. (2021). Local scour around tandem square porous piles in steady current. Ocean Engineering, 236: 109554. https://doi.org/10.1016/j.oceaneng.2021.109554

NOMENCLATURE

Q	discharge, m³/s
V	mean flow velocity, m/s
h	flow depth, m
D	pier diameter, m
ν	kinematic viscosity, m²/s
Re_h	Reynolds number
Fr	Froude number
$d_{s,\max}$	maximum scour depth, m or cm
R_d	maximum scour-depth reduction, %
V_s	scour volume, m³ or cm³
R_V	scour-volume reduction, %
Δz	bed-elevation change, m or cm
R_A	positive bed-elevation area ratio, %